Analytic Morse/long-range potential energy surfaces and predicted infrared spectra for CO_2-H_2

Hui Li, Pierre-Nicholas Roy, and Robert J. Le Roy[a)]
Department of Chemistry, University of Waterloo, Waterloo, Ontario N2L 3G1, Canada

(Received 12 February 2010; accepted 21 April 2010; published online 7 June 2010)

Five-dimensional *ab initio* potential energy surfaces (PESs) for CO_2-H_2 that explicitly incorporate dependence on the Q_3 asymmetric-stretch normal-mode coordinate of the CO_2 monomer and are parametrically dependent on its Q_1 symmetric-stretch coordinate have been calculated. Analytic four-dimensional PESs are obtained by least-squares fitting vibrationally averaged interaction energies for $v_3(CO_2)=0$, and 1 to the Morse/long-range potential function form. These fits to 23 113 points have root-mean-square (rms) deviations of 0.143 and 0.136 cm^{-1}, and require only 167 parameters. The resulting vibrationally averaged PESs provide good representations of the experimental infrared data: for infrared transitions of *para*- and *ortho*-H_2-CO_2, the rms discrepancies are only 0.004 and 0.005 cm^{-1}, respectively. The calculated infrared band origin shifts associated with the ν_3 fundamental of CO_2 are -0.179 and -0.092 cm^{-1} for *para*-H_2-CO_2 and *ortho*-H_2-CO_2, in good agreement with the (extrapolated) experimental values of -0.198 and -0.096 cm^{-1}. © *2010 American Institute of Physics*. [doi:10.1063/1.3428619]

I. INTRODUCTION

Liquid ^{4}He and ^{3}He are the only substances that are known to exhibit superfluidity, and there is considerable interest in finding superfluidity in other materials.[1] Like ^{4}He atoms, para-H_2 molecules are spinless indistinguishable bosons, so they might also be expected to show superfluid behavior at low temperatures.[2] Recent spectroscopic studies of molecules embedded in helium droplets[3–11] suggest that a possible route for investigating superfluidity of parahydrogen (p-H_2) is to consider p-H_2 clusters doped with a single chromophore molecule such as HCN, HF, CO, OCS, N_2O, or CO_2.[12–16] An accurate description of binary complexes is an essential starting point for the exploration of larger clusters, as quantum Monte Carlo simulations of doped He clusters are known to be very sensitive to the quality of the pair potentials utilized for the simulations.[17,18]

Since the first infrared spectrum of CO_2-H_2 complexes in the region of the strong v_3 fundamental band of CO_2 was recorded by McKellar,[19] two theoretical studies of this complex have been reported.[20,21] One was based on a four-dimensional (4D) potential energy surface (PES) with CO_2 fixed at its equilibrium geometry;[20] however, although a 4D treatment may be adequate for describing the microwave spectrum of a ground-state species, it cannot properly describe infrared spectra involving excitation of an intramolecular CO_2 vibrational mode. The other was a five-dimensional (5D) *ab initio* potential which explicitly took account of the v_3 asymmetric-stretch vibrational motion of rigidly linear CO_2 while the symmetric-stretch Q_1 coordinate was fixed at a value defined by the experimental ground-state inertial rotational constant B_0.[21] However, recent results of quantum Monte Carlo simulations of $CO_2(He)_n$ clusters show that the symmetric-stretch coordinate Q_1 may *not* be ignored when predicting the ν_3 band-origin shifts for CO_2 in van der Waals clusters.[18] Moreover, the "working form" of the first of these PESs involves cubic spline interpolation over the three angles and use of the interpolating moving least-squares method for the intermolecular separation R,[20] while that for the second was defined by fits to sums of products of linear and exponential angular terms at each pair of R and Q_3 values, combined with spline interpolation over those two coordinates.[21] Neither of those approaches yields a readily "portable" functional form, or defines the PES in terms of parameters with real physical significance, and neither incorporates the correct theoretically known inverse-power long-range behavior.

Recently, Le Roy *et al.* introduced the "Morse/long-range" (MLR) radial potential function form which incorporates theoretically known long-range inverse-power behavior within a single smooth and flexible analytic function.[22,23] For atom-molecule or molecule-molecule systems, allowing parameters of that radial function to vary with angle and monomer-stretching coordinate yields a compact and flexible multidimensional functional form. Application of this approach to the CO_2-He system yielded a function that explicitly incorporates the Q_3 asymmetric-stretch vibrational motion of CO_2 and has the correct angle-dependent inverse-power long-range behavior.[24,18] Vibrationally averaging over Q_3 for different vibrational levels of the CO_2 monomer yielded analogous two-dimensional (2D) forms and led to remarkably accurate predictions of the vibrational frequency shifts of CO_2 in $(He)_n$ for cluster sizes up to $n=40$.[18]

In the present work, 4D versions of such MLR functions (depending on three angles and R) have been fitted to vibrationally averaged interaction energies obtained from new 5D *ab initio* PESs for CO_2-H_2 which explicitly incorporate the Q_3 asymmetric-stretch vibrational motion of CO_2, but are

[a)]Electronic mail: leroy@uwaterloo.ca.

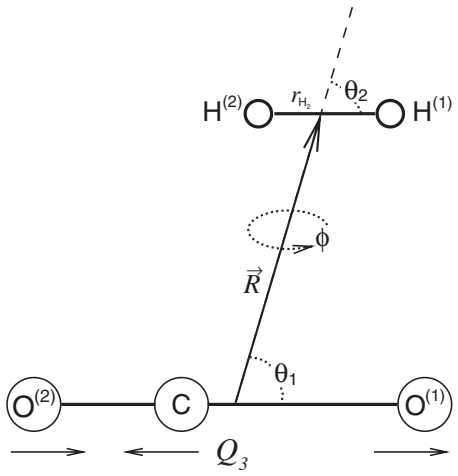

FIG. 1. Jacobi coordinates for the CO_2-H_2 complex.

associated with different values of the symmetric-stretch coordinate Q_1. The new *ab initio* calculations and the techniques used for computing the eigenvalues of the resulting PES are described in Sec. II. Section III then presents our analytic 4D potential function form and describes its fit to the *ab initio* results, while Sec. IV presents predictions of the infrared and microwave spectra for the CO_2-H_2 bimer implied by this surface and compares them with experiment.

II. COMPUTATIONAL METHODS

A. *Ab initio* calculations

The geometry of a CO_2-H_2 complex in which CO_2 is rigidly linear can be described naturally using the Jacobi coordinates $(R,\theta_1,\theta_2,\phi,Q_3)$ shown in Fig. 1; there, $\vec{R}$ is a vector pointing from the center of mass of CO_2 to the center of mass of H_2, θ_1, the angle between $\vec{R}$, and a vector pointing from atom $O^{(2)}$ to atom $O^{(1)}$, θ_2, the angle between $\vec{R}$, and a vector pointing from $H^{(2)}$ atom to $H^{(1)}$, ϕ, the dihedral angle between the two planes defined by $\vec{R}$, with the CO_2 molecule and with H_2, and $Q_3=(r_{CO}^{[1]}-r_{CO}^{[2]})/\sqrt{2}$ is the normal mode coordinate for the ν_3 antisymmetric stretch vibration of CO_2. In all of these calculations, the bond length of the H_2 molecule was fixed at the average value for the ground state, $r_{H_2}\equiv\langle r\rangle_{0,0}=0.766\,639\,3$ Å.[25] Our recent work on CO_2-He showed that when the asymmetric-stretch mode of CO_2 is excited, the effect of the associated change in the average value of the symmetric stretch coordinate $Q_1=(r_{CO}^{[1]}+r_{CO}^{[2]})/\sqrt{2}$ cannot be ignored.[18,24] Hence, in our *ab initio* calculations for the CO_2-H_2 complex, the sum of the two C–O bond lengths was fixed at twice the average bond lengths implied by the experimental moments of inertia for the ground state $(v_1,v_2,v_3)=(0,0,0)$, and the first excited asymmetric-stretch level of CO_2, (0,0,1).

In a full six-dimensional treatment which also took account of the symmetric stretch coordinate Q_1, the total potential energy for CO_2-H_2 would be written as

$$V(R,\theta_1,\theta_2,\phi,Q_3,Q_1)=V_{CO_2}(Q_3,Q_1)+\Delta V(R,\theta_1,\theta_2,\phi,Q_3,Q_1), \quad (1)$$

in which $V_{CO_2}(Q_3,Q_1)$ is the effective 2D potential energy for the symmetric and asymmetric stretching of an isolated, rigidly linear CO_2 molecule, and $\Delta V(R,\theta_1,\theta_2,\phi,Q_3,Q_1)$ is the intermolecular interaction potential. However, our recent results for the CO_2-He system showed that a reduced-dimension treatment with the symmetric stretch coordinate Q_1 fixed at its average values for the appropriate v_3 vibrational level of CO_2 was a good approximation which led to very accurate predicted vibrational frequency shifts for CO_2 in $(He)_n$ clusters.[18,24] Following that approach, our effective 5D potentials for CO_2-H_2 can be defined as

$$\langle\psi_{v_1}^{\{v_3\}}(Q_1)|V(R,\theta_1,\theta_2,\phi,Q_3,Q_1)|\psi_{v_1}^{\{v_3\}}(Q_1)\rangle \approx V(R,\theta_1,\theta_2,\phi,Q_3;\bar{Q}_1^{\{v_3\}}) = V_{CO_2}(Q_3;\bar{Q}_1^{\{v_3\}})+\Delta V(R,\theta_1,\theta_2,\phi,Q_3;\bar{Q}_1^{\{v_3\}}), \quad (2)$$

in which the notation reminds us that the average value of Q_1 depends on the asymmetric-stretch vibrational quantum number v_3.

The CO_2 monomer geometry and hence the effective one-dimensional (1D) potentials $V_{CO_2}(Q_3;\bar{Q}_1^{\{v_3\}})$ governing both the Q_3 vibration of a free CO_2 monomer and the intermolecular potential $\Delta V(R,\theta_1,\theta_2,\phi,Q_3;\bar{Q}_1^{\{v_3\}})$ depend not only on Q_3, but also on the associated (fixed) value of the symmetric stretch coordinate $\bar{Q}_1^{\{v_3\}}$. The average values of the C–O bond length in the ground $(v_1,v_2,v_3)=(0,0,0)$ and (0,0,1) excited states of CO_2 implied by the experimental moments of inertia are known to be $r_0=1.162\,086$ and 1.166 695 Å, respectively.[26] Our taking account of this difference differs from the approach used in recent 5D treatments of CO_2-H_2 and of N_2O-H_2, in which the same fixed Q_1 value was used to define the effective 1D monomer stretching potentials when treating states of the complex associated with the ground $(v_3=0)$ and first excited $(v_3=1)$ levels of the chromophore.[21,27]

The effective 1D potentials $V_{CO_2}(Q_3;\bar{Q}_1^{\{v_3\}})$ governing the Q_3 vibration of the isolated CO_2 monomer were calculated using single- and double-excitation coupled-cluster theory with a noniterative perturbation treatment of triple excitations [CCSD(T)].[28] The basis set used was the augmented correlation-consistent quadruple-zeta (aug-cc-pVQZ) basis set of Woon and Dunning,[29] and counterpoise corrections were applied. For a chosen fixed value for the sum of the two C–O bond lengths, the potential energy was computed at 29 values of Q_3 ranging from 0.0 to 0.5 Å, and those values were fitted to an even-power polynomial expansion:

$$V_{CO_2}(Q_3;\bar{Q}_1^{\{v_3\}})=\sum_{n=0(2)} a_n(\bar{Q}_1^{\{v_3\}})Q_3^n. \quad (3)$$

The coefficients of the polynomial expansions used to represent the 1D effective CO_2 asymmetric-stretch potentials are presented in Table I of Ref. 24.

The intermolecular potential energies of CO_2-H_2 were calculated at the [CCSD(T)]/aug-cc-pVTZ level, supple-

mented with an additional set of bond functions $(3s3p2d1f1g)$ (where $\alpha=0.9,0.3,0.1$ for $3s$ and $3p$; $\alpha=0.6,0.2$, for $2d$; $\alpha=0.3$ for f and g) placed at the midpoint of the intermolecular axis R.[30,31] The supermolecule approach was used to produce the intermolecular potential energy $\Delta V(R,\theta_1,\theta_2,\phi,Q_3;\bar{Q}_1^{\{v_3\}})$, which is defined as the difference between the energy of the CO_2-H_2 complex and the sum of the energies of the CO_2 and H_2 monomers. The full counterpoise procedure was employed to correct for basis set superposition error.[32] All calculations were carried out using the MOLPRO package.[33]

Some 41 148 symmetry-unique *ab initio* points were calculated for both the ground $(v_3=0)$ and first excited $(v_3=1)$ states, with Q_1 fixed at the values $\bar{Q}_1^{\{v_3\}}$ defined by the experimental inertial rotational constants for the (0,0,0) and (0,0,1) levels of CO_2. The calculations were performed on regular grids for all five degrees of freedom. Five grid points corresponding to $Q_3=-0.115\,863$, $-0.054\,977$, 0.0, 0.054 977, and 0.115 863 Å were chosen for the CO_2 stretching coordinate, while a relatively dense grid of 26 points ranging from 2.2 to 12.0 Å was used for the R intermolecular coordinate. The angular coordinates θ_1 and θ_2 range from 0° to 180° with step sizes of 15°, and the dihedral angle φ ranges from 0° to 90° at intervals of 30°. This yielded two effective 5D *ab initio* PESs, for which the lists of symmetry-unique points may be obtained from the journal's online data archive.[34]

B. Hamiltonian and reduced-dimension treatment

Within the Born–Oppenheimer approximation, without separating the intra- and intermolecular vibrations, the rovibrational Hamiltonian of the CO_2-H_2 complex in the space-fixed frame has the form (in a.u.):[35–37]

$$\hat{H}=-\frac{1}{2\mu}\frac{\partial^2}{\partial R^2}-\frac{1}{2M}\frac{\partial^2}{\partial Q_3^2}+\frac{\hat{l}_1^2}{2I_{CO_2}}+B_{H_2}\hat{l}_2^2+\frac{(\hat{J}-\hat{l}_1-\hat{l}_2)^2}{2\mu R^2}+V(R,\theta_1,\theta_2,\phi,Q_3;\bar{Q}_1^{\{v_3\}}), \tag{4}$$

in which $\mu^{-1}=(2m_H)^{-1}+(2m_O+m_C)^{-1}$ and $M=m_Cm_O/(2m_O+m_C)$, where m_H, m_C, and m_O are the masses of the H, C, and O atoms,[38] respectively, B_{H_2} is the inertial rotational constant of H_2, $I_{CO_2}\equiv I(Q_3;\bar{Q}_1^{\{v_3\}})$ is the moment of inertia of an isolated CO_2 molecule, and $V(R,\theta_1,\theta_2,\phi,Q_3;\bar{Q}_1^{\{v_3\}})$ is the total potential energy of the system.

The above Hamiltonian incorporates full coupling between the intermolecular and Q_3 vibrations. However, convergence of the eigenvalue calculations is very slow at the high internal energies associated with excitation of the ν_3 vibration of CO_2, since it requires a relatively large number of Lanczos iterations.[21,24] It is therefore highly desirable to separate the treatment of the inter- and intramolecular motions. Since the ν_3 vibrational mode of CO_2 has a much higher frequency than do the intermolecular modes, Born–Oppenheimer separation type arguments suggest that it should be a good approximation to introduce such a separation, as long as the off-diagonal vibrational coupling is sufficiently small.[21,24] In this approximation, the total vibrational wave function would be written as the product

$$\Psi_{v_3}(R,\theta_1,\theta_2,\phi,Q_3;\bar{Q}_1^{\{v_3\}})=\phi^{\{v_3\}}(R,\theta_1,\theta_2,\phi)\psi_v(Q_3;\bar{Q}_1^{\{v_3\}}), \tag{5}$$

in which v_3 is the quantum number for a specific asymmetric-stretch vibrational state of the free CO_2 molecule, and the associated 1D vibrational wave function $\psi_v(Q_3;\bar{Q}_1^{\{v_3\}})$ is obtained by solving the 1D Schrödinger equation:

$$\left[\frac{-1}{2M}\frac{d^2}{dQ_3^2}+V_{CO_2}(Q_3;\bar{Q}_1)\right]\psi_v(Q_3;\bar{Q}_1)=E_v\psi_v(Q_3;\bar{Q}_1). \tag{6}$$

The present work focuses on complexes formed from CO_2 in the ground $(v_3=0)$ and first excited $(v_3=1)$ asymmetric stretch states of CO_2. Using Eq. (5), the vibrationally averaged CO_2-H_2 interaction potential for CO_2 in vibrational level v_3 is

$$\bar{V}^{\{v_3\}}(R,\theta_1,\theta_2,\phi)=\int_{-\infty}^{\infty}\psi_{v_3}^*(Q_3;\bar{Q}_1^{\{v_3\}})\Delta V(R,\theta_1,\theta_2,\phi,Q_3;\bar{Q}_1^{\{v_3\}})\times\psi_{v_3}(Q_3;\bar{Q}_1^{\{v_3\}})dQ_3, \tag{7}$$

and the associated 4D intermolecular Hamiltonian in the space-fixed reference frame is

$$\hat{H}=-\frac{1}{2\mu}\frac{\partial^2}{\partial R^2}+B_{CO_2}^{v_3}\hat{l}_1^2+B_{H_2}^{v}\hat{l}_2^2+\frac{(\hat{J}-\hat{l}_1-\hat{l}_2)^2}{2\mu R^2}+\bar{V}^{\{v_3\}}(R,\theta_1,\theta_2,\phi), \tag{8}$$

in which

$$B_{CO_2}^{v_3}=\left\langle\psi_{v_3}\left|\frac{1}{2I(Q_3;\bar{Q}_1^{\{v_3\}})}\right|\psi_{v_3}\right\rangle \tag{9}$$

is the CO_2 inertial rotational constant and $I(Q_3;\bar{Q}_1^{\{v_3\}})$ is the instantaneous CO_2 moment of inertia. Note that the vibrationally averaged intermolecular potentials $\bar{V}^{\{v_3\}}(R,\theta_1,\theta_2,\phi)$ for different values of v_3 differ because the 5D PESs being averaged over are associated with different values of $\bar{Q}_1^{\{v_3\}}$, and because the wave functions $\psi_{v_3}(Q_3)$ are associated with different values of v_3, and because they were obtained from effective 1D potentials associated with different values of $\bar{Q}_1^{\{v_3\}}$.

In order to solve our 4D Schrödinger equation numerically in terms of the body-fixed angles (θ_1,θ_2,ϕ), the Hamiltonian in the body-fixed reference frame is written as[39–42]

$$\hat{H}=\hat{T}_{str}+\hat{T}_{diag}+\hat{T}_{off}+\hat{T}_{Cor}+\bar{V}^{\{v_3\}}(R,\theta_1,\theta_2,\phi), \tag{10}$$

in which

$$\hat{T}_{str}=-\frac{1}{2\mu}\frac{\partial^2}{\partial R^2}, \tag{11}$$

$$\hat{T}_{\rm diag} = -\left(\frac{1}{2\mu R^2} + B^{v_3}_{\rm CO_2}\right)\left[\frac{\partial^2}{\partial\theta_1^2} + \cot\theta_1\frac{\partial}{\partial\theta_1} - \frac{1}{\sin^2\theta_1}(\hat{J}_z - \hat{l}_{2z})^2\right] + \left[\frac{1}{2\mu R^2} + B_{\rm H_2}\right]\hat{l}_2^2 + \frac{1}{2\mu R^2}[\hat{J}^2 - 2(\hat{J}_z - \hat{l}_{2z})^2 - 2\hat{J}_z\hat{l}_{2z}], \quad (12)$$

$$\hat{T}_{\rm off} = \frac{1}{2\mu R^2}[\hat{l}_{2+}\hat{a}_1^- + \hat{l}_{2-}\hat{a}_1^+], \quad (13)$$

$$\hat{T}_{\rm Cor} = -\frac{1}{2\mu R^2}[\hat{J}_-\hat{a}_1^+ + \hat{J}_+\hat{a}_1^- + \hat{J}_-\hat{l}_{2+} + \hat{J}_+\hat{l}_{2-}], \quad (14)$$

where

$$\hat{J}_\pm = \hat{J}_x \pm i\hat{J}_y, \quad \hat{l}_{2\pm} = \hat{l}_{2x} \pm i\hat{l}_{2y}, \quad (15)$$

$$\hat{a}_1^\pm = \pm\frac{\partial}{\partial\theta_1} - \cot\theta_1(\hat{J}_z - \hat{l}_{2z}). \quad (16)$$

Here, the operators $\widehat{J_x}$, $\widehat{J_y}$, and $\widehat{J_z}$ are the components of the total angular momentum operator $\hat{J}$ in the body-fixed frame, the z axis of the body-fixed frame lies along the Jacobi radial vector $\vec{R}$, and its x axis is in the plane that contains $\vec{R}$ and the CO_2 molecule. The above Hamiltonian contains full vibration-rotation coupling.

C. Basis function and matrix elements

A discrete variable representation (DVR) grid[43] was used for the radial part of the 4D Schrödinger equation. The angular part was then treated using parity-adapted rovibrational basis functions, which are linear combinations of the functions

$$\langle\theta_1,\theta_2,\phi;\alpha,\beta,\gamma|l_1l_2m;JKM\rangle = \sqrt{\frac{2J+1}{8\pi^2}}\Theta^{K-m}_{l_1}(\theta_1)Y^m_{l_2}(\theta_2,\phi)D^{J^*}_{MK}(\alpha,\beta,\gamma), \quad (17)$$

in which l_1 and l_2 are the total angular momentum quantum numbers for free rotation of the CO_2 and H_2 moities, respectively,

$$Y^m_{l_2}(\theta_2,\phi) = \frac{1}{\sqrt{2\pi}}\Theta^m_{l_2}(\theta_2)e^{im\phi}$$

are the familiar spherical harmonics, Θ^m_l is the normalized associated Legendre functions with the $(-1)^m$ Condon–Shortley phase factor,[44] and D^J_{MK} are the Wigner functions.[44] The body-fixed frame is related to the space-fixed frame via a rotation by the three Euler angles (α,β,γ). The projection of the total angular momentum $\vec{J}$ onto the space-fixed or body-fixed frame is given by M or K quantum numbers. The effect of the parity operator $\hat{E}^*$ on rovibrational functions is given by

$$\hat{E}^*|l_1l_2mK;JM\rangle = (-1)^J|l_1l_2-mK;JM\rangle, \quad (18)$$

so the parity-adapted basis functions can be written as

$$|l_1l_2mK;JMP\rangle = \frac{1}{\sqrt{(2+2\delta_{m,0}\delta_{K,0})}}\{|l_1l_2mK;JM\rangle + (-1)^{J+P}|l_1l_2-mK;JM\rangle\}, \quad (19)$$

where for $K>0$, $P=0$ and 1 correspond to even and odd parities, respectively. If $K=0$, the constraint that $m\geq 0$ is applied, and the combination $m=K=0$ and $(-1)^{J+P}=-1$ is not allowed.

In the parity-adapted angular finite basis representation (FBR), the kinetic energy terms have simple matrix elements. The diagonal matrix elements are

$$\langle l_1l_2mK;JMP|\hat{T}_{\rm diag}|l_1l_2mK;JMP\rangle = B_{\rm CO_2}l_1(l_1+1) + B^v_{\rm H_2}l_2(l_2+1) + \frac{1}{2\mu R^2}[J(J+1) + l_1(l_1+1) + l_2(l_2+1) - 2K^2 + 2m(K-m)], \quad (20)$$

and the three types of off-diagonal matrix elements are

$$\langle l_1l_2m+1K;JMP|\hat{T}_{\rm off}|l_1l_2mK;JMP\rangle = \frac{\sqrt{1+\delta_{m,0}\delta_{K,0}}}{2\mu R^2}\lambda^-_{l_1,K-m}\lambda^+_{l_2,m}, \quad (21)$$

$$\langle l_1l_2mK+1;JMP|\hat{T}_{\rm Cor}|l_1l_2mK;JMP\rangle = -\frac{\sqrt{1+\delta_{m,0}\delta_{K,0}}}{2\mu R^2}\lambda^+_{l_1,K-m}\lambda^+_{J,K}, \quad (22)$$

$$\langle l_1l_2m+1K+1;JMP|\hat{T}_{\rm Cor}|l_1l_2mK;JMP\rangle = -\frac{\sqrt{1+\delta_{m,0}\delta_{K,0}}}{2\mu R^2}\lambda^+_{l_2,m}\lambda^+_{J,K}, \quad (23)$$

with two special cases

$$\langle l_1l_2-m1;JMP|\hat{T}_{\rm Cor}|l_1l_2m0;JMP\rangle = \frac{-(-1)^{J+P}}{2\mu R^2}\lambda^-_{l_1,K-m}\lambda^-_{J,0}(m>0), \quad (24)$$

$$\langle l_1l_2-m+11;JMP|\hat{T}_{\rm Cor}|l_1l_2m0;JMP\rangle = \frac{-(-1)^{J+P}}{2\mu R^2}\lambda^-_{l_2,m}\lambda^-_{J,0}(m>0). \quad (25)$$

For the potential part, the matrix elements are not diagonal in the angular FBR basis. However, they could be calculated in the grid representation by applying a three-dimensional transformation[37] for the angles θ_1, θ_2, and φ, respectively, in which the potential energy matrix is diagonal. These integrals need first the application of a transformation from the parity-adapted FBR to the DVR basis, then multiplication by a diagonal potential matrix, and finally to be transformed back.[37,41] Gauss–Legendre quadrature was used for both the θ_1 and θ_2 angles, and Gauss–Chebyshev quadratures of the first kind and second kind were used to integrate φ for even and odd parity cases, respectively. The

Lanczos algorithm was then used to calculate the rovibrational energy levels by recursively diagonalizing the resulting discretized Hamiltonian matrix.[45]

III. ANALYTIC POTENTIAL ENERGY SURFACE FOR CO_2-H_2

A. Potential energy function

The vibrational-averaged *ab initio* intermolecular potential energies $\bar{V}^{\{v_3\}}(R,\theta_1,\theta_2,\phi)$, for CO_2-H_2 obtained from Eq. (7), were fitted to a generalization of the MLR potential function form,[23,46] which is written as

$$\bar{V}_{\mathrm{MLR}}(R,\theta_1,\theta_2,\phi) = \mathfrak{D}_e(\theta_1,\theta_2,\phi)\times\left\{-1+\left[1-\frac{u_{\mathrm{LR}}(R,\theta_1,\theta_2,\phi)}{u_{\mathrm{LR}}(R_e,\theta_1,\theta_2,\phi)}e^{-\beta(R,\theta_1,\theta_2,\phi)\cdot y_p^{\mathrm{eq}}(R,\theta_1,\theta_2,\phi)}\right]^2\right\}, \quad (26)$$

in which $\mathfrak{D}_e(\theta_1,\theta_2,\phi)$ is the depth and $R_e\equiv R_e(\theta_1,\theta_2,\phi)$ is the position of the minimum on a radial cut through the potential for angles $\{\theta_1,\theta_2,\phi\}$, while $u_{\mathrm{LR}}(R,\theta_1,\theta_2,\phi)$ is a function which defines the (attractive) limiting long-range behavior of the effective 1D potential along that cut as

$$\bar{V}(R,\theta_1,\theta_2,\phi)\simeq\mathfrak{D}_e(\theta_1,\theta_2,\phi)-u_{\mathrm{LR}}(R,\theta_1,\theta_2,\phi)+\cdots. \quad (27)$$

Because both H_2 and CO_2 are nonpolar, an appropriate functional form for $u_{\mathrm{LR}}(R,\theta_1,\theta_2,\phi)$ is

$$u_{\mathrm{LR}}(R,\theta_1,\theta_2,\phi)=\frac{\bar{C}_5(\theta_1,\theta_2,\phi)}{R^5}+\frac{\bar{C}_6(\theta_1,\theta_2,\phi)}{R^6}+\frac{\bar{C}_8(\theta_1,\theta_2,\phi)}{R^8}, \quad (28)$$

in which the long-range coefficients $\bar{C}_n$ have also been averaged over the CO_2 asymmetric-stretch coordinate Q_3, and the denominator factor $u_{\mathrm{LR}}(R_e,\theta_1,\theta_2,\phi)$ is that same function evaluated at $R=R_e(\theta_1,\theta_2,\phi)$. The radial distance variable in the exponent in Eq. (26) is the dimensionless quantity

$$y_p^{\mathrm{eq}}(R,\theta_1,\theta_2,\phi)=\frac{R^p-R_e(\theta_1,\theta_2,\phi)^p}{R^p+R_e(\theta_1,\theta_2,\phi)^p}, \quad (29)$$

where p is a small positive integer which must be greater than the difference between the largest and smallest (inverse) powers appearing in Eq. (28), $p>(8-5)$,[23] and the exponent coefficient function $\beta(R,\theta_1,\theta_2,\phi)$ is a (fairly) slowly varying function of R, which is written as the constrained polynomial

$$\beta(R,\theta_1,\theta_2,\phi)=y_p^{\mathrm{ref}}(R,\theta_1,\theta_2,\phi)\beta_\infty(\theta_1,\theta_2,\phi)+[1-y_p^{\mathrm{ref}}(R,\theta_1,\theta_2,\phi)]\times\sum_{i=0}^{N}\beta_i(\theta_1,\theta_2,\phi)y_q^{\mathrm{ref}}(R,\theta_1,\theta_2,\phi)^i, \quad (30)$$

whose behavior is defined in terms of the two new radial variables:

$$y_p^{\mathrm{ref}}(R,\theta_1,\theta_2,\phi)=\frac{R^p-R_{\mathrm{ref}}^p}{R^p+R_{\mathrm{ref}}^p}\quad\text{and}\quad y_q^{\mathrm{ref}}(R,\theta_1,\theta_2,\phi)=\frac{R^q-R_{\mathrm{ref}}^q}{R^q+R_{\mathrm{ref}}^q}, \quad (31)$$

in which $R_{\mathrm{ref}}\equiv f_{\mathrm{ref}}\times R_e(\theta_1,\theta_2,\phi)$. Although most previous work with this model was performed using a single radial variable to define the exponent coefficient function $\beta(R,\theta_1,\theta_2,\phi)$ (i.e., with $q=p$) and with $R_{\mathrm{ref}}=R_e$, (i.e., with $f_{\mathrm{ref}}=1$), it has recently been shown that use of $f_{\mathrm{ref}}>1$, and of a separate smaller power $q<p$, to define the radial variable in the power-series portion of Eq. (30) can lead to more compact and robust potential functions.[46] In the potential function model used in the present work, $p=4$, $q=3$, and $f_{\mathrm{ref}}=1.5$.

The definition of $y_p^{\mathrm{eq}}(R,\theta_1,\theta_2,\phi)$ and the algebraic structure of Eqs. (26) and (30) mean that

$$\lim_{R\to\infty}\beta(R,\theta_1,\theta_2,\phi)=\lim_{R\to\infty}\{\beta(R,\theta_1,\theta_2,\phi)\cdot y_p^{\mathrm{eq}}(R,\theta_1,\theta_2,\phi)\}\equiv\beta_\infty(\theta_1,\theta_2,\phi)=\ln\{2\mathfrak{D}_e(\theta_1,\theta_2,\phi)/u_{\mathrm{LR}}(R_e,\theta_1,\theta_2,\phi)\}. \quad (32)$$

The parameters $\mathfrak{D}_e(\theta_1,\theta_2,\phi)$, $R_e(\theta_1,\theta_2,\phi)$, and the various exponent expansion coefficients $\beta_i(\theta_1,\theta_2,\phi)$, all are expanded in the form

$$F(\theta_1,\theta_2,\phi)=\sum_{l_1,l_2,l}F_{l_1l_2l}A_{l_1l_2l}(\theta_1,\theta_2,\phi), \quad (33)$$

in which $F=\mathfrak{D}_e$, R_e or β_i, $\phi=\phi_1-\phi_2$, and l is the label associated with the vector sum of l_1 and l_2 and has the range of values $|l_1-l_2|\le l\le|l_1+l_2|$. These three indices must also satisfy the restrictions that all of l_1, l_2, and l_1+l_2+l must be even, because both CO_2 and H_2 have centers of symmetry. The angular basis functions appearing here are defined as

$$A_{l_1l_2l}(\theta_1,\theta_2,\phi)=\sum_{m=-l_{\min}}^{l_{\min}}\begin{pmatrix}l_1 & l_2 & l\\ m & -m & 0\end{pmatrix}C_{l_1,m}(\theta_1,\phi_1)C_{l_2,-m}(\theta_2,\phi_2), \quad (34)$$

in which $C_{l,m}(\theta,\phi)=[4\pi/(2l+1)]^{1/2}Y_{l,m}(\theta,\phi)$ are the spherical harmonic functions defined with Racah normalization,[47] the quantity in large brackets is the Wigner $3j$ factor,[48] and $l_{\min}=\min(l_1,l_2)$.

The presence of permanent quadrupole moments on CO_2 and H_2 means that the leading term in the expression for $u_{\mathrm{LR}}(R,\theta_1,\theta_2,\phi)$ is the electrostatic quadrupole-quadrupole interaction,[49] whose (vibrationally averaged) coefficient may be written as

TABLE I. Expansion coefficients $\bar{\mathfrak{D}}_e^{l_1,l_2,l}$[cm^{-1}] defining our 4D vibrationally averaged PES for $^{12}C\ ^{16}O_2(v_3=0)-H_2$.

$\bar{\mathfrak{D}}_e^{0,0,0}$	77.548	$\bar{\mathfrak{D}}_e^{0,2,2}$	−40.2	$\bar{\mathfrak{D}}_e^{0,4,4}$	1.63	$\bar{\mathfrak{D}}_e^{0,6,6}$	−0.48
$\bar{\mathfrak{D}}_e^{2,0,2}$	−91.82	$\bar{\mathfrak{D}}_e^{2,2,0}$	23.03	$\bar{\mathfrak{D}}_e^{2,4,2}$	−45.0	$\bar{\mathfrak{D}}_e^{2,6,4}$	0.61
$\bar{\mathfrak{D}}_e^{4,0,4}$	94.86	$\bar{\mathfrak{D}}_e^{2,2,2}$	38.79	$\bar{\mathfrak{D}}_e^{2,4,4}$	7.4	$\bar{\mathfrak{D}}_e^{2,6,6}$	−0.4
$\bar{\mathfrak{D}}_e^{6,0,6}$	−64.98	$\bar{\mathfrak{D}}_e^{2,2,4}$	460.77	$\bar{\mathfrak{D}}_e^{2,4,6}$	5.3	$\bar{\mathfrak{D}}_e^{2,6,8}$	0.5
$\bar{\mathfrak{D}}_e^{8,0,8}$	39.23	$\bar{\mathfrak{D}}_e^{4,2,2}$	−26.01	$\bar{\mathfrak{D}}_e^{4,4,0}$	60.6	$\bar{\mathfrak{D}}_e^{4,6,2}$	−0.31
$\bar{\mathfrak{D}}_e^{10,0,10}$	−22.19	$\bar{\mathfrak{D}}_e^{4,2,4}$	10.56	$\bar{\mathfrak{D}}_e^{4,4,2}$	−2.53	$\bar{\mathfrak{D}}_e^{4,6,4}$	0.2
$\bar{\mathfrak{D}}_e^{12,0,12}$	7.79	$\bar{\mathfrak{D}}_e^{4,2,6}$	−239.78	$\bar{\mathfrak{D}}_e^{4,4,4}$	1.5	$\bar{\mathfrak{D}}_e^{4,6,8}$	0.5
		$\bar{\mathfrak{D}}_e^{6,2,4}$	21.21	$\bar{\mathfrak{D}}_e^{4,4,6}$	−3.8	$\bar{\mathfrak{D}}_e^{4,6,10}$	−0.8
		$\bar{\mathfrak{D}}_e^{6,2,6}$	−10.9	$\bar{\mathfrak{D}}_e^{4,4,8}$	−47.5	$\bar{\mathfrak{D}}_e^{6,6,0}$	0.11
		$\bar{\mathfrak{D}}_e^{6,2,8}$	11.6	$\bar{\mathfrak{D}}_e^{6,4,2}$	2.1	$\bar{\mathfrak{D}}_e^{6,6,2}$	−0.1
		$\bar{\mathfrak{D}}_e^{8,2,6}$	−14.9	$\bar{\mathfrak{D}}_e^{6,4,4}$	−1.1	$\bar{\mathfrak{D}}_e^{6,6,6}$	−0.2
		$\bar{\mathfrak{D}}_e^{8,2,8}$	6.7	$\bar{\mathfrak{D}}_e^{6,4,6}$	2.2	$\bar{\mathfrak{D}}_e^{6,6,10}$	−0.16
		$\bar{\mathfrak{D}}_e^{8,2,10}$	−63.5	$\bar{\mathfrak{D}}_e^{6,4,10}$	−1.7	$\bar{\mathfrak{D}}_e^{6,6,12}$	−0.37
		$\bar{\mathfrak{D}}_e^{10,2,8}$	14.6	$\bar{\mathfrak{D}}_e^{8,4,4}$	18.9		
		$\bar{\mathfrak{D}}_e^{10,2,10}$	−4.5	$\bar{\mathfrak{D}}_e^{8,4,6}$	−3.0		
		$\bar{\mathfrak{D}}_e^{10,2,12}$	26.4	$\bar{\mathfrak{D}}_e^{8,4,8}$	1.6		
		$\bar{\mathfrak{D}}_e^{12,2,10}$	−13.7	$\bar{\mathfrak{D}}_e^{8,4,10}$	−2.2		
		$\bar{\mathfrak{D}}_e^{12,2,12}$	2.2	$\bar{\mathfrak{D}}_e^{8,4,12}$	2.4		
				$\bar{\mathfrak{D}}_e^{10,4,6}$	2.9		
				$\bar{\mathfrak{D}}_e^{10,4,8}$	−0.9		
				$\bar{\mathfrak{D}}_e^{10,4,10}$	0.5		
				$\bar{\mathfrak{D}}_e^{10,4,12}$	2.4		
				$\bar{\mathfrak{D}}_e^{12,4,8}$	2.9		
				$\bar{\mathfrak{D}}_e^{12,4,10}$	−0.9		
				$\bar{\mathfrak{D}}_e^{12,4,12}$	0.5		

$$\bar{C}_5(\theta_1,\theta_2,\phi) = -(3\sqrt{70})\bar{Q}_{H_2}\bar{Q}_{CO_2}A_{224}(\theta_1,\theta_2,\phi), \tag{35}$$

in which $\bar{Q}_{H_2}$ and $\bar{Q}_{CO_2}$ are the vibrationally averaged quadrupole moments of ground-state H_2 and CO_2.[50,51] Our v_3-dependent values of $\bar{Q}_{CO_2}$ were obtained by averaging over the Q_3-dependence of the quadrupole moment function reported by Haskopoulos and Maroulis.[51]

The vibrationally averaged dispersion coefficients $\bar{C}_{6(8)}\times(\theta_1,\theta_2,\phi)$ may be expanded as

$$\bar{C}_{6(8)}(\theta_1,\theta_2,\phi) = \sum_{l_1 l_2 l} \bar{C}_{6(8)}^{l_1 l_2 l} A_{l_1 l_2 l}(\theta_1,\theta_2,\phi).$$

An experimental value of the leading totally isotropic coefficient $\bar{C}_{6,\mathrm{exp}}^{000}$ has been obtained from dipole oscillator strength distributions by Jhanwar and Meath,[52] but no angle- or stretching-dependent long-range coefficients have been reported for this system. Estimates of the dispersion coefficients for $(l_1,l_2,l)\neq(0,0,0)$, were therefore obtained from the geometric-mean averages $\bar{C}_{6(8),\mathrm{gm}}^{l_1 l_2 l}$ of the analogous coefficients for the CO_2-CO_2 and H_2-H_2 interactions.[53,54] Our final values of the coefficients for these angle-dependent terms were then obtained by scaling these calculated "geometric-mean" coefficients by the ratios of the "experimental" to the geometric-mean isotropic C_6 coefficients:

$$\bar{C}_{6(8)}^{l_1 l_2 l} = \bar{C}_{6(8),\mathrm{gm}}^{l_1 l_2 l} \times (\bar{C}_{6,\mathrm{exp}}^{000}/\bar{C}_{6,\mathrm{gm}}^{000}). \tag{36}$$

Since our *ab initio* 5D PES incorporates the Q_3 asymmetric-stretch normal-mode coordinate of the CO_2 monomer, the Van der Waals interaction will also include induction terms. Following Buckingham,[55] the coefficient of the R^{-6} induction term was taken to be

$$\bar{C}_{6,\mathrm{ind}}(\theta_1,\theta_2,\phi) = \sum_{l_1 l_2 l} \bar{C}_{6,\mathrm{ind}}^{l_1 l_2 l} A_{l_1 l_2 l}(\theta_1,\theta_2,\phi)$$
$$= \overline{[\mu_{CO_2}(Q_3)]^2} \times \Bigg[\alpha_{H_2}^{\mathrm{av}}(A_{000}+\sqrt{5}A_{202}) + (\alpha_{H_2}^{\parallel}-\alpha_{H_2}^{\perp})\left(\frac{\sqrt{5}}{3}A_{022}+\frac{3}{\sqrt{5}}A_{220} - \frac{\sqrt{10}}{\sqrt{7}}A_{222}+\frac{2\sqrt{2}}{\sqrt{35}}A_{224}\right)\Bigg], \tag{37}$$

in which the leading factor on the right hand side is the vibrational average of the square of the instantaneous CO_2 dipole moment, while $\alpha_{H_2}^{\parallel}$, $\alpha_{H_2}^{\perp}$, and $\alpha_{H_2}^{\mathrm{av}}$ are, respectively, the parallel, perpendicular, and isotropic-average polarizabilities of H_2. The latter were defined by the vibrationally averaged values for ground-state H_2 reported by Bishop and Cheung,[56] while the former was calculated using the Q_3-dependent CO_2 dipole moment reported by Haskopoulos and Maroulis.[51]

Finally, while the v_3-dependence of the angle-dependent dispersion terms was neglected, that for the leading isotropic coefficient was assumed to scale as the isotropic average polarizability of CO_2 $\alpha_{CO_2}^{\mathrm{av}}(Q_3)=[\alpha_{CO_2}^{\parallel}(Q_3)+2\alpha_{CO_2}^{\perp}(Q_3)]/3$. Using the Q_3-dependent polarizabilities for CO_2 reported by Haskopoulos and Maroulis,[51] this yields

$$\bar{C}_{6,\mathrm{disp}}^{000}(v_3=1) = \bar{C}_{6,\mathrm{disp}}^{000}(v_3=0) \times \frac{\langle\psi_{v_3=1}|\alpha_{CO_2}^{\mathrm{av}}(Q_3)|\psi_{v_3=1}\rangle}{\langle\psi_{v_3=0}|\bar{\alpha}_{CO_2}^{\mathrm{av}}(Q_3)|\psi_{v_3=0}\rangle}. \tag{38}$$

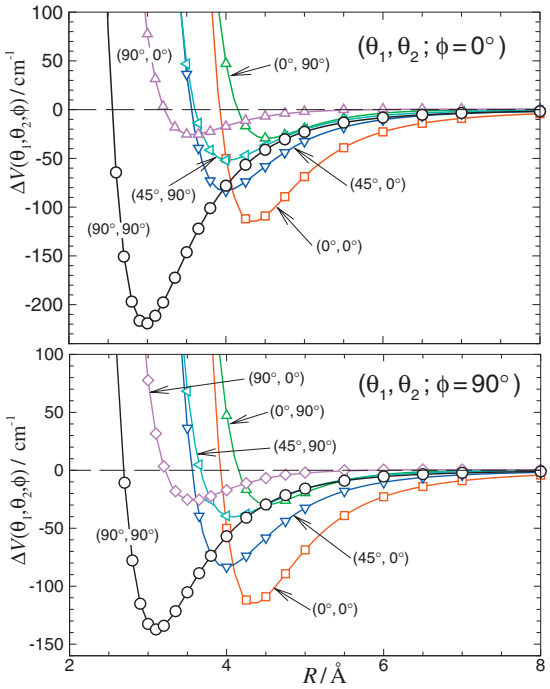

FIG. 2. Vibrational averaged *ab initio* interaction energies (points) along cuts through the analytic 4D PES for CO_2-H_2 at various relative orientations.

B. Least-squares fits

To commence any nonlinear least-squares fit, it is necessary to have realistic initial trial values of the fitting parameters. In the present case of fits to the 4D-MLR form of Eq. (26), they were obtained in the following manner. First, a fit to the ordinary 1D MLR form (depending only on R) was performed for all distinct combinations of θ_1, θ_2, and ϕ, using program betaFIT.[57] This involved some experimentation to ascertain the most appropriate choice for the integer parameters p and q and the factor f_{ref} appearing in the definitions of the radial variables $y_p^{\text{eq}}(R;\theta_1,\theta_2,\phi)$, $y_p^{\text{ref}}(R;\theta_1,\theta_2,\phi)$, and $y_q^{\text{ref}}(R;\theta_1,\theta_2,\phi)$ of Eqs. (29) and (31), and for the order N of the exponent polynomial of Eq. (30). As was pointed out above, the present potential function model used $p=4$, $q=3$, and $f_{\text{ref}}=1.5$, and the exponent polynomial order was $N=5$. The resulting values of $\mathfrak{D}_e(\theta_1,\theta_2,\phi)$, $R_e(\theta_1,\theta_2,\phi)$, and $\beta_i(\theta_1,\theta_2,\phi)$ (for $i=0-N$) were then fitted to Eq. (33), and the resulting expansion coefficients $F_{l_1 l_2 l}$ used as starting parameters in the global 4D fits of the vibrationally averaged potential energies to Eq. (26).

In the final fits, the input *ab initio* energies were weighted by assigning uncertainties of $u_i=0.1$ cm^{-1} to points in the attractive well region where $V(R,\theta_1,\theta_2,\phi) \le 0.0$ cm^{-1}, and $u_i=[V(R,\theta_1,\theta_2,\phi)+10.0]/100.0$ cm^{-1}, to those in the repulsive wall region where $V(R,\theta_1,\theta_2,\phi) > 0.0$ cm^{-1}. Using these weights, our final 167-parameters fits to the 23 113 vibrationally averaged interaction energies below 1000 cm^{-1} yielded dimensionless rms residual discrepancies of only 1.43 and 1.36 for $v_3=0$ and $v_3=1$, respectively. For data points in the well region, $V(R,\theta_1,\theta_2,\phi)<0$, this corresponds to rms discrepancies of 0.143 and 0.141 cm^{-1}, respectively. Over one-third of (63/167) of those fitting parameters are required to define $\mathfrak{D}_e(\theta_1,\theta_2,\phi)$ (see Table I), 42 to define $R_e(\theta_1,\theta_2,\phi)$, and 31, 15, 4, 4, 3, and 5 to define $\beta_i(\theta_1,\theta_2,\phi)$ for $i=0-5$, respectively. Our use of the sequential rounding and refitting procedure of Ref. 58 means that the parameter sets are relatively compact (e.g., see Table I). The resulting sets of potential parameters and a FORTRAN subroutine for generating these potentials may be obtained from the authors or from the journal's supplementary data archive.[34]

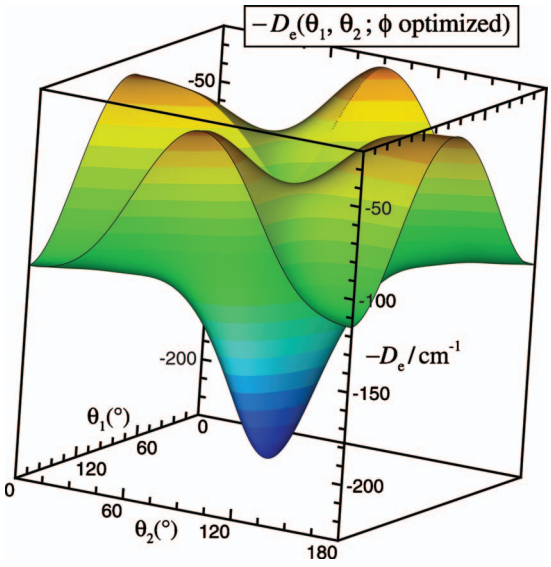

FIG. 3. Minimum energy on our vibrationally averaged 4D PES for $CO_2(v_3=0)-H_2$ as a function of angles θ_1 and θ_2, for optimized values of ϕ and R.

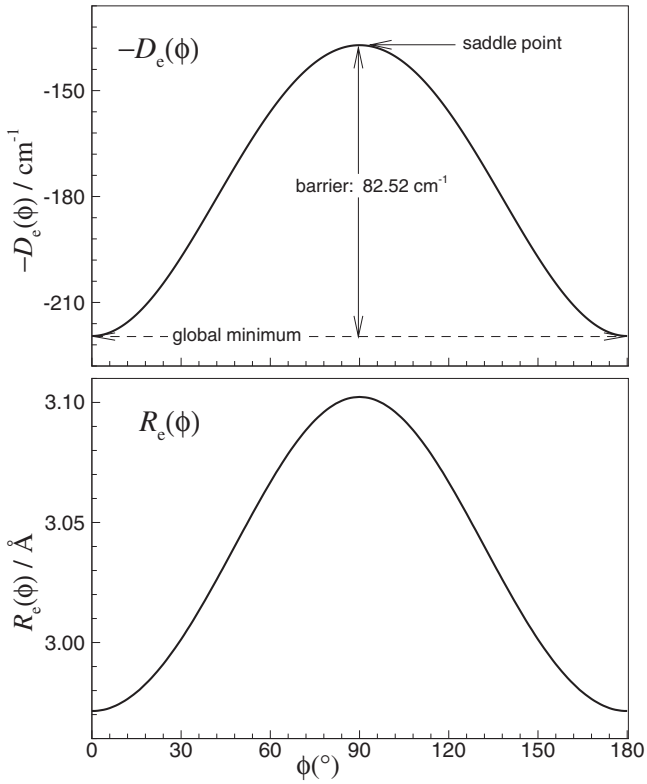

FIG. 4. Energies (upper) and radial positions (lower) along the ϕ-rotation isomerization path between global minima on our vibrationally averaged 4D PES for $CO_2(v_3=0)-H_2$.

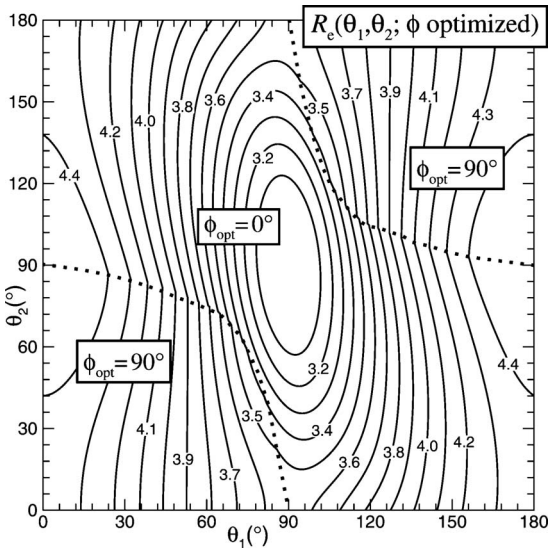

FIG. 5. Radial positions of the minimum on our vibrationally averaged 4D PES for $CO_2(v_3=0)-H_2$ as a function of angles θ_1 and θ_2, for optimized values of ϕ and R.

IV. RESULTS AND DISCUSSION

A. Features of the four-dimensional potential energy surface

Figure 2 illustrates the behavior of our potential along some cuts through our 4D PES for $v_3=0$. Figure 3 then shows how the well depth of our fitted, vibrationally averaged, 4D PES for $CO_2(v_3=0)-H_2$ depends on θ_1 and θ_2 when ϕ is optimized to minimize the energy for each (θ_1,θ_2). The complex structure seen there indicates why so many parameters (63) are required to represent $\mathfrak{D}_e(\theta_1,\theta_2,\phi)$ accurately. The global minima well depth of 219.65 cm^{-1} occurs at the parallel geometry $\theta_1=\theta_2=90°$ with $R=2.970$ Å and $\phi=0°$ (and by symmetry, $\phi=180°$). Figure 4 illustrates the nature of the lowest-energy isomerization pathway, which is a rotation along the ϕ coordinate with $\theta_1=\theta_2=90°$ with a barrier of height 82.36 cm^{-1} located at $R=3.102$ Å. Figure 3 also shows that in the (θ_1,θ_2) domain, equivalent global minima are separated by four equivalent saddle points with energies of -114.91 cm^{-1} at collinear geometries where $R=4.342$ Å and θ_1 and θ_2 are equal to either 0° or 180°. It also shows that there are two types of minimum energy paths joining these saddle points to global minima. The first is a barrierless path along which the H_2 and CO_2 monomers remain coplanar $(\varphi=0)$ and θ_1 increases while θ_2 decreases (or vice versa), so that relative to $\vec{R}$, each rotates through 90° in a direction counter to the rotation of the other as they move to a collinear arrangement. The second is a path with a barrier of height 162.58 cm^{-1} along which both θ_1 and θ_2 increase (or decrease) in concert; the transition state on this path is located at $R=3.786$ Å and $\phi=90°$, for either $\theta_1=59.3°$ and $\theta_2=45.3°$, or $\theta_1=120.7°$ and $\theta_2=134.7°$.

Figure 5 shows how the radial positions of the minimum energy depend on θ_1 and θ_2 when ϕ is optimized at every point. The dotted curves seen there indicate configurations at which the optimum value of ϕ switches abruptly between 0° and 90°. As may be expected, contours which cross these dotted curves show small discontinuities at these switchover points. Nonetheless, the fact that the structure seen here is somewhat simpler than that seen in Fig. 3 indicates why the description of $R_e(\theta_1,\theta_2,\phi)$ requires only about 2/3 as many parameters (42 versus 63) as are required to define $\mathfrak{D}_e(\theta_1,\theta_2,\phi)$. One of the nice features of the generalized MLR form is the fact that these two physically meaningful quantities, $\mathfrak{D}_e(\theta_1,\theta_2,\phi)$ and $R_e(\theta_1,\theta_2,\phi)$, which are directly determined by the fit, incorporate most of the basic structural information about our 4D surfaces.

The geometries and energies of the global minimum and the saddle points separating them are summarized in Table II; those for $v_3=0$ are in good agreement with these features of a previous *ab initio* surface for this system calculated by Ran *et al.*,[21] but differ somewhat from those of the potential calculated by Wang *et al.*[20] For the vibrationally averaged excited-state $(v_3=1)$ surface, the contour plots look almost the same as those for the ground state $(v_3=0)$, and, as shown in Table II, the positions and energies of the stationary points are shifted only slightly.

B. Bound states and band origin shifts

The rovibrational energy levels of CO_2-H_2 were calculated using the radial DVR and parity-adapted angular FBR methods described in Sec. II B and II C. Because of the symmetry properties associated with P, l_1, and l_2, there exist eight symmetry blocks, and the rovibrational energy levels for each block could be calculated separately. An 80-point

TABLE II. Properties of stationary points of the CO_2-H_2 PES and comparisons with results for previously reported surfaces. All entries are given as $\{R[\text{Å}],\theta_1^\circ,\theta_2^\circ,\phi^\circ,\bar{V}[\text{cm}^{-1}]\}$.

	Global minimum	ϕ-rotation saddle point[a]	Reference
4D-MLR($v_3=0$)	{2.970, 90.0, 90.0, 0.0, −219.65}	{3.102, 90.0, 90.0, 90.0, −137.13}	Present
4D-MLR($v_3=1$)	{2.972, 90.0, 90.0, 0.0, −219.26}	{3.104, 90.0, 90.0, 90.0, −136.96}	Present
$Q_3=0$	{2.970, 90.0, 90.0, 0.0, −219.68}	{3.100, 90.0, 90.0, 90.0, −137.27}	21
$Q_3=0$	{2.978, 90.0, 90.0, 0.0, −211.93}	{2.978, 90.0, 90.0, 90.0, −122.55}	20
	Collinear saddle point	θ_1/θ_2-rotation saddle point[b]	
4D-MLR($v_3=0$)	{4.342, 0.0, 0.0, 0.0, −114.91}	{3.786, 59.3, 45.3, 90.0, −57.07}	Present
4D-MLR($v_3=1$)	{4.346, 0.0, 0.0, 0.0, −114.62}	{3.785, 59.4, 45.5, 90.0, −57.46}	Present

[a]Lowest energy barrier between equivalent minima, see text.
[b]Saddle point between global minimum and collinear minimum, see text.

TABLE III. Energies (in cm^{-1}) for vibrational levels of our vibrationally averaged 4D-MLR PESs for CO_2-H_2 expressed relative to the relevant asymptote, with assigned vibrational quantum labels given in parentheses (n_s,n_b,l_2,p_{m_2}), compared to published results for some previously reported surfaces. Entries in the first row for each case are for the $CO_2(v_3=0)$ complex and those in the second row for $CO_2(v_3=1)$, while Δv_0 is the band origin shift.

		Para-H_2-CO_2				*Ortho*-H_2-CO_2			
Parity	l_1	(n_s,n_b,l_2,p_{m_2})	Present	Reference 21	Reference 20	(n_s,n_b,l_2,p_{m_2})	Present	Reference 21	Reference 20
		(0,0,0,0)	−54.437	−54.390	−50.383	(0,1,1,1)	−50.990	−49.884	−46.472
			−54.616	−54.504			−51.210	−50.021	
		(0,2,0,0)	−25.392	−25.525	−23.544	(0,3,1,1)	−38.228	−37.323	−35.693
			−25.660	−25.651			−38.433	−37.443	
	Even	(0,4,0,0)	−17.113	−17.237	−15.116	(0,3,1,0)	−28.492	−27.929	−25.547
			−17.405	−17.376			−28.752	−28.047	
		(1,0,0,0)	−5.058	−5.052	−3.335	(0,1,1,0)	−22.231	−21.002	−18.368
			−5.242	−5.132			−22.523	−21.138	
		(0,6,0,0)	−0.756	−0.722					
			−0.912	−0.790					
$P=0$		(1,1,0,0)	−0.161						
			−0.163						
		(0,1,0,0)	−31.013	−31.118	−28.316	(0,0,1,1)	−77.633	−76.303	−71.704
			−31.272	−31.248			−77.725	−76.402	
	Odd	(0,3,0,0)	−22.006	−22.214	−20.235	(0,2,1,0)	−40.916	−39.842	−37.837
			−22.303	−22.365			−41.129	−39.951	
		(0,5,0,0)	−9.046	−9.157	−7.107	(0,2,1,1)	−34.830	−33.875	−31.789
			−9.371	−9.285			−35.055	−34.006	
						(1,0,1,0)	−22.276	−21.237	−19.099
							−22.525	−21.331	
	Even					(0,1,1,−1)	−29.049	−27.523	−24.993
							−29.295	−27.627	
$P=1$									
						(0,0,1,−1)	−56.312	−55.030	−51.068
							−56.458	−55.117	
	Odd					(1,0,1,−1)	−19.538		−16.172
							−19.788		
Δv_0		Theory	−0.179	−0.113			−0.092	−0.099	
		Experiment	−0.198				−0.096		

sine-DVR grid with points ranging from 3.0 to 20.0 bohr was used for the radial (R) stretching coordinate, and 27 and 19 associated Legendre basis functions were used for the angular coordinates θ_1 and θ_2, respectively. The integration over θ_1 and θ_2 used 32 and 24 Gauss–Legendre quadrature points, respectively, and that over ϕ used 52 equally spaced points in the range $[0, 2\pi]$.

Table III lists the energies of the $(J=0)$ intermolecular vibrational energy levels of $CO_2(v_3=0)-H_2$ and $CO_2(v_3=1)-H_2$ on our 4D-MLR surfaces and compares them to published results for previously reported surfaces.[20,21] It is known that the rotation of H_2 in the complex is dominated by $l_2=0$, terms for *para*-H_2 and by $l_2=1$, for *ortho*-H_2, due to the large spacings between the rotational energy levels of molecular hydrogen. However, the small rotational level spacings of CO_2 mean that the quantum label l_1 is best replaced by a θ_1-bending quantum label n_b. The rovibrational energy levels may then be labeled by the six quantum numbers: v_3, J, n_s, n_b, l_2, and p_{m_2}, where v_3 is the asymmetric stretch quantum number of CO_2, J is the total angular momentum, n_s is the Van der Waals vibrational stretch quantum numbers, and p_{m_2} is a composite index giving the parity of the state.[20] Following the approach of Ref. 59, our calculations for *para*-H_2-CO_2 complexes used an effective H_2-molecule inertial rotational constant B_{H_2} calculated from the experimental $l_2=0\rightarrow2$, level spacing, while our *ortho*-H_2-CO_2 calculations used a value of B_{H_2} defined by the $l_2=1\rightarrow3$ monomer level spacing.

For *para*-H_2-CO_2, our surface supports nine bound vibrational levels for complexes formed from either ground-state $(v_3=0)$ or excited $(v_3=1)$ CO_2, and the level energies for those two cases are very similar to one another. The present surface for this species supports one more level than was reported for the surface of Ref. 21 and two more than does the PES of Ref. 20. The zero-point energy on our ground-state $(v_3=0)$ surface is 165.213 cm^{-1}, about 3/4 of the global well depth, a result which is very similar to that of Ref. 21 (165.29 cm^{-1}), but somewhat larger than that of Ref. 20 (161.549 cm^{-1}).

For the *ortho*-H_2-CO_2 complex, whose level energies are expressed relative to the $j_{H_2}=1$, dissociation channel, we find a total of 27 bound intermolecular vibrational states with energies lower than its asymptote (at[59] $2B_{H_2}=118.486\ 75$ cm^{-1}), three times more than were found for the *para*-H_2-CO_2 complex. Because of the strong mixing of

TABLE IV. Infrared transition energies (in cm^{-1}) of *para*-H_2–CO_2($v_3=0\rightarrow1$) calculated from our vibrationally averaged 4D MLR PESs and comparisons with experiment and with previous theoretical predictions.

		Present		Reference 21	
Levels $J'_{K'_aK'_c}-J''_{K''_aK''_c}$	Obs.	Calc.	Diff.	Calc.	Diff.
Frequencies relative to the 2349.1433 cm^{-1} band origin of CO_2					
$1_{01}-0_{00}$	0.456	0.472	0.016	0.549	0.093
$1_{10}-1_{11}$	−0.049	−0.030	0.019	0.045	0.094
$2_{12}-1_{11}$	0.953	0.968	0.015	1.049	0.096
$1_{01}-2_{02}$	−1.479	−1.457	0.022	−1.381	0.098
$2_{21}-2_{02}$		1.554		1.631	
$2_{21}-2_{20}$		−0.225		−0.146	
$3_{03}-2_{02}$	1.611	1.623	0.012	1.716	0.105
$3_{21}-2_{02}$		3.663		3.758	
$3_{21}-2_{20}$		1.884		1.981	
$1_{10}-2_{11}$	−1.663	−1.644	0.019	−1.569	0.094
$2_{12}-2_{11}$		−0.646		−0.566	
$3_{12}-2_{11}$	1.939	1.955	0.016	2.057	0.118
$2_{12}-3_{13}$		−1.902		−1.822	
$4_{14}-3_{13}$	2.030	2.041	0.011	2.144	0.114
Average			0.017		0.102
RMSD			0.017		0.102
Frequencies relative to the 2348.9452 cm^{-1} band origin of *para*-H_2–CO_2					
$1_{01}-0_{00}$	0.654	0.652	−0.002	0.662	0.008
$1_{10}-1_{11}$	0.149	0.149	0.000	0.158	0.009
$2_{12}-1_{11}$	1.151	1.147	−0.004	1.162	0.011
$1_{01}-2_{02}$	−1.281	−1.278	0.003	−1.268	0.013
$2_{21}-2_{02}$		1.733		1.744	
$2_{21}-2_{20}$		−0.045		−0.033	
$3_{03}-2_{02}$	1.809	1.802	−0.007	1.829	0.020
$3_{21}-2_{02}$		3.843		3.871	
$3_{21}-2_{20}$		2.064		2.094	
$1_{10}-2_{11}$	−1.465	−1.465	0.000	−1.456	0.009
$2_{12}-2_{11}$		−0.467		−0.453	
$3_{12}-2_{11}$	2.137	2.134	−0.003	2.170	0.033
$2_{12}-3_{13}$		−1.723		−1.709	
$4_{14}-3_{13}$	2.228	2.221	−0.007	2.257	0.029
Average			−0.002		0.017
RMSD			0.004		0.020

angular and radial functions, making $\{n_s,n_b\}$ assignments based on the nodal structures of the wave functions becomes increasingly difficult with increasing energy, and Table III lists only the lowest 11 assigned vibrational levels; a listing of all 27 level energies is included in the supplemental data.[34] As seen in Table III, the ground state of *ortho*-H_2–CO_2 is bound by −77.633 and −77.725 cm^{-1} for $v_3=0$ and $v_3=1$, respectively, which makes this species some 23 cm^{-1} more stable than is *para*-H_2–CO_2, a result consistent with previous results.[20,21]

As shown in the last two rows of Table III, the calculated band origin shifts predicted by our 4D-MLR surfaces are $\Delta v_0=-0.179$ and −0.092 cm^{-1} for *para*-H_2–CO_2 and *ortho*-H_2–CO_2, respectively, results in very good agreement with the experimental values of −0.198 and −0.096 cm^{-1}.[19] The analogous predictions of Ref. 21 are −0.113 and −0.099 cm^{-1}, respectively. Since the *ab initio* calculations of Ref. 21 were performed using a very similar level of theory, we speculate that the relatively large discrepancy for *para*-H_2–CO_2 is probably due to their neglect of the effect of the change in the average value of Q_1 on excitation of the ν_3 mode. The relatively better agreement for *ortho*-H_2–CO_2 is consistent with a finding from our work on the He–CO_2 system that neglect of the effect of changes in $\bar{Q}_1$ becomes increasingly serious at geometries farther from equilibrium, a consideration which becomes particularly important in treatments of larger clusters.[18,24]

C. Predicted Infrared Spectra

Infrared $v_3=0\rightarrow1$, transition energies calculated from our vibrationally averaged 4D PESs for *para*-H_2–CO_2 and *ortho*-H_2–CO_2 are listed and compared with experiment and with previous theoretical predictions in Tables IV and V, respectively. The transitions shown there are all for complexes which remain in their ground intermolecular vibra-

TABLE V. Infrared transition energies (in cm^{-1}) of *ortho*-$H_2-CO_2(v_3=0\rightarrow 1)$ calculated from our vibrationally averaged 4D MLR PESs and comparisons with experiment and with previous theoretical predictions.

		Present		Reference 21	
Levels $J'_{K'_aK'_c}-J''_{K''_aK''_c}$	Obs.	Calc.	Diff.	Calc.	Diff.
Frequencies relative to the 2349.1433 cm^{-1} band origin of CO_2					
$0_{00}-1_{01}$	−0.720	−0.715	0.005	−0.722	−0.002
$2_{02}-1_{01}$	1.123	1.123	0.000	1.128	0.005
$1_{11}-1_{10}$	−0.213	−0.210	0.003	−0.214	−0.001
$2_{11}-1_{10}$	1.256	1.256	0.000	1.263	0.007
$1_{11}-2_{12}$	−1.231	−1.223	0.008	−1.228	0.003
$2_{11}-2_{12}$	0.238	0.243	0.005	0.249	0.011
$3_{13}-2_{12}$	1.574	1.572	−0.002	1.583	0.009
$2_{20}-2_{21}$	−0.083	−0.079	0.004	−0.078	0.005
$3_{22}-2_{21}$	1.751	1.749	−0.002	1.761	0.010
$2_{02}-3_{03}$	−1.907	−1.897	0.010	−1.893	0.014
$3_{22}-3_{03}$	1.865	1.911	**0.047**	1.921	**0.056**
$4_{04}-3_{03}$	2.196	2.191	−0.004	2.218	0.022
$2_{11}-3_{12}$	−2.144	−2.135	0.009	−2.129	0.015
$4_{13}-3_{12}$	2.545	2.542	−0.003	2.579	0.034
$4_{22}-3_{21}$	2.501	2.512	0.011	2.546	0.045
$3_{13}-4_{14}$	−2.348	−2.336	0.012	−2.327	0.021
RMSD (including $3_{22}-3_{03}$)			0.014		0.023
RMSD (excluding $3_{22}-3_{03}$)			0.007		0.018
Frequencies relative to the 2349.0473 cm^{-1} band origin of *ortho*-H_2-CO_2					
$0_{00}-1_{01}$	−0.625	−0.623	0.002	−0.623	0.002
$2_{02}-1_{01}$	1.218	1.215	−0.003	1.227	0.009
$1_{11}-1_{10}$	−0.118	−0.118	0.000	−0.115	0.003
$2_{11}-1_{10}$	1.351	1.348	−0.003	1.362	0.011
$1_{11}-2_{12}$	−1.136	−1.131	0.005	−1.129	0.007
$2_{11}-2_{12}$	0.333	0.335	0.002	0.348	0.015
$3_{13}-2_{12}$	1.669	1.664	−0.005	1.682	0.013
$2_{20}-2_{21}$	0.012	0.013	0.001	0.021	0.009
$3_{22}-2_{21}$	1.846	1.841	−0.005	1.860	0.014
$2_{02}-3_{03}$	−1.812	−1.805	0.007	−1.794	0.018
$3_{22}-3_{03}$	1.960	2.003	**0.043**	2.020	**0.060**
$4_{04}-3_{03}$	2.291	2.283	−0.008	2.317	0.026
$2_{11}-3_{12}$	−2.049	−2.043	0.006	−2.030	0.019
$4_{13}-3_{12}$	2.640	2.634	−0.006	2.678	0.038
$4_{22}-3_{21}$	2.596	2.604	0.008	2.645	0.049
$3_{13}-4_{14}$	−2.253	−2.244	0.009	−2.228	0.025
RMSD (including $3_{22}-3_{03}$)			0.012		0.026
RMSD (excluding $3_{22}-3_{03}$)			0.005		0.021

tional level ($n_s=0$). The rotational levels of these complexes were assigned using the conventional asymmetric-rotor labels J, K_a, and K_c, where J is the total angular momentum and K_a and K_c denote the projections of J onto the a and c principal axes of inertia. Due to the interchange symmetry of the indistinguishable zero-spin ^{16}O nuclei, the allowed rotational states for $C^{16}O_2$ in its the ground state ($v_3=0$) only have even values of the angular momentum quantum number l_1, while for the first excited asymmetric-stretch state ($v_3=1$) state only odd values of l_1 are allowed.[20] Hence, for *para*-H_2-CO_2, the allowed rotational levels have $(K_a,K_c)=$(even,even), or (odd, odd) for the CO_2 ground state ($v_3=0$), and $(K_a,K_c)=$(even,odd), or (odd, even) for the excited state ($v_3=1$). Similarly, for *ortho*-H_2-CO_2, the allowed rotational levels have $(K_a,K_c)=$(even,odd) or (odd, even) for $v_3=0$, and $(K_a,K_c)=$(even,even), or (odd, odd) when $v_3=1$.

The upper part of Table IV expresses the infrared transition energies of *para*-H_2-CO_2 relative to the ν_3 fundamental band origin of CO_2. Column 3 shows the transition energies yielded by our vibrationally averaged 4D PESs, which are seen to agree very well with the experimental values shown in column 2.[19] The differences seen in column 4 are very small and the fact that the average and rms discrepancies are very similar shows that most of these differences are due to the 0.019 cm^{-1} error in our calculated band origin shift. If the experimental and calculated transition energies are expressed to their respective band origins, we obtain the results seen in the lower half of Table IV. As is seen in the

lower half of column 4, the differences with experiment[19] are then significantly reduced, yielding average and rms discrepancies of only -0.002 and 0.004 cm^{-1}, respectively. The results presented in columns 5 and 6 show that our surfaces yield approximately five times better agreement with experiment than do the predictions of Ref. 21.

For *ortho*-H_2-CO_2, the calculated infrared transition frequencies expressed relative to the band origin of free CO_2 are given in the upper part of Table V. Again, column 2 lists the experimental results from Ref. 19 and column 3 the values calculated from our vibrationally averaged 4D PESs. The differences seen in column 4 are very small except for the transition $3_{22}-3_{03}$ (shown in bold font), for which the discrepancy of 0.047 cm^{-1} is anomalously large relative to the rms discrepancy of 0.007 cm^{-1} for the others. If the infrared transitions are expressed relative to the band origin for the *ortho*-H_2-CO_2 complex, as shown in the lower part of Table V, the discrepancy of 0.043 cm^{-1} for the $3_{22}-3_{03}$ transition remains anomalously large relative to the rms discrepancy of 0.005 cm^{-1} for the others. Although their overall agreement with experiment is roughly a factor of 3 worse than ours, this anomaly is also evident in the predictions of Ref. 21. This led us to speculate that there might have been an error in the assignment of this experimental datum.

To address this question, our calculations for both the *para*- and *ortho*-H_2-CO_2 complexes were extended to higher J, and predictions were generated for all possible transitions in the neighborhood of the observed line at 2351.008 cm^{-1}, with the simulated transition energies being based on combining the level energies on our upper and lower PESs with the experimental band origin energies. The portion of those results shown in Table VI shows that there are no other transitions of *ortho*-H_2-CO_2 which could account for the line that had been assigned[19] as the $3_{22}-3_{03}$ transition of *ortho*-H_2-CO_2, but that it is coincident with our prediction for the $3_{21}-2_{20}$ transition of *para*-H_2-CO_2. Thus, we conclude that the this apparent anomaly in our *para*-H_2-CO_2 predictions is most likely due to the presence of a small amount of *para*-H_2-CO_2 impurity in the *ortho*-H_2-CO_2 experiment which led to a misassignment of this transition.

TABLE VI. Predicted infrared transition energies for *ortho*-H_2-CO_2 and *para*-H_2-CO_2 near the observed line at 2351.008 cm^{-1}, as generated from our vibrationally averaged 4D MLR PES, comparison with experiment.

$J'_{K'_aK'_c}-J''_{K''_aK''_c}$	Obs.	Calc.
	Ortho-H_2-CO_2	
$4_{13}-4_{14}$		2350.153
$2_{02}-1_{01}$	2350.266	2350.263
$2_{11}-1_{10}$	2350.399	2350.397
$3_{13}-2_{12}$	2350.717	2350.711
$3_{22}-2_{21}$	2350.894	2350.889
$3_{22}-3_{03}$	**2351.008**	2351.051
$6_{15}-6_{16}$		2351.242
$4_{04}-3_{03}$	2351.339	2351.331
$5_{24}-5_{05}$		2351.409
$4_{31}-3_{30}$		2351.529
$4_{22}-3_{21}$	2351.644	2351.652
$4_{13}-3_{12}$	2351.688	2351.682
$5_{15}-4_{14}$		2351.756
$5_{24}-4_{23}$		2352.055
$5_{42}-4_{41}$		2352.098
$5_{33}-4_{32}$		2352.131
$5_{33}-5_{14}$		2352.181
$2_{20}-1_{01}$		2352.243
$6_{06}-5_{05}$		2352.291
$3_{31}-3_{12}$		2352.564
$6_{51}-5_{50}$		2352.646
$6_{42}-5_{41}$		2352.718
$6_{15}-5_{14}$		2352.827
$6_{33}-5_{32}$		2352.854
$6_{24}-5_{23}$		2353.026
$4_{22}-3_{03}$		2353.774
$5_{42}-5_{23}$		2354.229
	Para-H_2-CO_2	
$2_{12}-3_{31}$		2343.342
$1_{01}-2_{20}$		2345.887
$3_{12}-3_{31}$		2345.943
$2_{21}-3_{22}$		2346.992
$3_{03}-3_{22}$		2347.061
$2_{12}-3_{13}$		2347.221
$1_{10}-2_{11}$	2347.480	2347.480
$1_{01}-2_{02}$	2347.664	2347.666
$2_{12}-2_{11}$		2348.478
$2_{21}-2_{20}$		2348.899
$3_{30}-3_{31}$		2348.939
$1_{10}-1_{11}$	2349.094	2349.093
$3_{21}-3_{22}$		2349.101
$1_{01}-0_{00}$	2349.599	2349.596
$3_{12}-3_{13}$		2349.822
$2_{12}-1_{11}$	2350.096	2350.091
$2_{21}-2_{02}$		2350.678
$3_{03}-2_{02}$	2350.754	2350.747
$3_{21}-2_{20}$		**2351.008**
$3_{12}-2_{11}$	2351.082	2351.079
$4_{14}-3_{13}$	2351.173	2351.165
$4_{23}-3_{22}$		2351.477
$4_{32}-3_{31}$		2351.528
$3_{21}-2_{02}$		2352.787
$3_{30}-2_{11}$		2354.075
$4_{32}-3_{13}$		2355.407
$4_{41}-3_{22}$		2356.588

V. DISCUSSION AND CONCLUSIONS

This paper presents accurate analytic vibrationally averaged 4D PESs for $H_2-CO_2(v_3)$ complexes for $v_3=0$ and 1 which were obtained from effective six-dimensional *ab initio* potential energies that explicitly incorporate the dependence of the interaction energy on both the Q_1 and Q_3 normal-mode coordinate of CO_2. The *ab initio* interaction energies were obtained at the CCSD(T) level using a large aug-cc-pVTZ basis set and with bond functions placed at the midpoint of the intermolecular axis. The vibrationally averaged potential energies were fitted to a 4D generalization of the MLR potential form which incorporates the correct theoretically known long-range inverse-power behavior;[22,23] having this correct long-range behavior is important if this potential is to provide a good description of a CO_2 molecule in medium to large sized $(H_2)_n$ clusters. The global 4D fit to the 23 113

interaction energies had a root-mean-square (rms) residual in the well region of only 0.143 and 0.136 cm^{-1} for $v_3=0$ and 1, respectively, and required only 167 fitting parameters.

The type of analytic potential energy function expression used here differs from the "damped electrostatic and dispersion attraction plus exponential repulsion" form used in much other work on van der Waals molecules.[21,27,47,53,60] While both types of functions may accurately represent such surfaces, we believe that the extended MLR form used here has significant advantages. In particular, it is explicitly defined in terms of two key physically interesting properties of the system, the well depth $\mathcal{D}_e(\theta_1,\theta_2,\phi)$ and the position of the radial minimum $R_e(\theta_1,\theta_2.\phi)$, and most of its fitting parameters (here, 105 out of 167) are involved in defining how those two properties depend on relative molecular orientations. Figures 3 and 5 illustrate the fact that considerable physical insight may be gained by characterizing potentials in this way. In contrast, all of the fitting parameters in the conventional forms are involved in characterizing exponential and pre-exponential product functions which cannot be readily related to any physical properties of the system. It is also noteworthy that the MLR-type functions may also be used for chemically bound systems, while "inverse-power attraction plus exponential repulsion" forms can only really be used for van der Waals systems. Moreover, while the version of the MLR form used here does not explicitly incorporate "damping" into the inverse-power terms, its effect is implicitly incorporated into the behavior of the exponent coefficient $\beta(R,\theta_1,\theta_2,\phi)$.

Rovibrational energy levels for *para*-H_2-CO_2 and *ortho*-H_2-CO_2 were obtained by the radial DVR/angular FBR method. Our potentials support 9 and 27 bound intermolecular vibrational states for *para*-H_2 and *ortho*-H_2-CO_2 complexes, respectively. The calculated band origin shifts associated with the ν_3 fundamental transition of CO_2 are -0.179 and -0.092 cm^{-1} for *para*-H_2-CO_2 and *ortho*-H_2-CO_2, respectively, which results in good agreement with the experimental values of -0.198 and -0.096 cm^{-1}. This suggests that these surfaces will yield reliable predictions for the ν_3 vibrational shifts of CO_2 in $(H_2)_n$ clusters. The calculated spectroscopic properties of our vibrationally averaged 4D PESs are in excellent agreement with experiment: for infrared transitions of *para*-H_2-CO_2 and *ortho*-H_2-CO_2, the rms discrepancies are 0.004 and 0.005 cm^{-1}, respectively. The accuracy of the present PESs allowed us to discern a probably misassignment of one of the reported experimental lines of *ortho*-H_2-CO_2.

One consideration entirely missing from the present discussion (and from all analogous previous work) is the possible effect of the CO_2 bending coordinate, Q_2. Within the context of an adiabatic separation of fast versus slow molecular motions, we believe that this is not a serious omission. In particular, the fact that the average structure is linear for both the (0,0,0) and (0,0,1) vibrational states of CO_2 suggests that this degree of freedom should not contribute significantly to the observed ν_3 band origin shifts for CO_2 in $CO_2-(H_2)_n$ clusters.[61] On the other hand, the nonzero average value of the square of the instantaneous perpendicular dipole moment will contribute a small additional induction term to the overall interaction energy. If this is slightly larger for $CO_2(v_3=1)$ than for $CO_2(v_3=0)$, it would affect the predicted ν_3 vibrational frequency shifts and might even explain the residual 10% discrepancy between the experimental and calculated shifts for this system. Work to examine this question is now under way.

[1] S. Grebenev, B. Sartakov, J. P. Toennies, and A. F. Vilesov, Science **289**, 1532 (2000).
[2] V. L. Ginzburg and A. A. Sobyanin, JETP Lett. **15**, 242 (1972).
[3] J. Tang and A. R. W. McKellar, J. Chem. Phys. **119**, 754 (2003).
[4] Y. Xu and W. Jäger, J. Chem. Phys. **119**, 5457 (2003).
[5] J. Tang and A. R. W. McKellar, J. Chem. Phys. **119**, 5467 (2003).
[6] J. Tang, A. R. W. McKellar, F. Mezzacapo, and S. Moroni, Phys. Rev. Lett. **92**, 145503 (2004).
[7] J. Tang and A. R. W. McKellar, J. Chem. Phys. **121**, 181 (2004).
[8] A. R. W. McKellar, J. Chem. Phys. **127**, 044315 (2007).
[9] A. R. W. McKellar, Y. Xu, and W. Jäger, J. Phys. Chem. A **111**, 7329 (2007).
[10] A. R. W. McKellar, J. Chem. Phys. **128**, 044308 (2008).
[11] L. A. Surin, A. V. Potapov, B. S. Dumesh, S. Schlemmer, Y. Xu, P. L. Raston, and W. Jäger, Phys. Rev. Lett. **101**, 233401 (2008).
[12] D. T. Moore and R. E. Miller, J. Chem. Phys. **119**, 4713 (2003).
[13] D. T. Moore and R. E. Miller, J. Phys. Chem. A **108**, 1930 (2004).
[14] S. Moroni, M. Botti, S. De Palo, and A. R. W. McKellar, J. Chem. Phys. **122**, 094314 (2005).
[15] J. Tang and A. R. W. McKellar, J. Chem. Phys. **121**, 3087 (2004).
[16] J. Tang and A. R. W. McKellar, J. Chem. Phys. **123**, 114314 (2005).
[17] S. Paolini, S. Fantoni, S. Moroni, and S. Baroni, J. Chem. Phys. **123**, 114306 (2005).
[18] H. Li, N. Blinov, P.-N. Roy, and R. J. Le Roy, J. Chem. Phys. **130**, 144305 (2009).
[19] A. R. W. McKellar, J. Chem. Phys. **122**, 174313 (2005).
[20] L. Wang, M. H. Yang, A. R. W. McKellar, and D. H. Zhang, Phys. Chem. Chem. Phys. **9**, 131 (2007).
[21] H. Ran, Y. Zhou, and D. Q. Xie, J. Chem. Phys. **126**, 204304 (2007).
[22] R. J. Le Roy, Y. Huang, and C. Jary, J. Chem. Phys. **125**, 164310 (2006).
[23] R. J. Le Roy and R. D. E. Henderson, Mol. Phys. **105**, 663 (2007).
[24] H. Li and R. J. Le Roy, Phys. Chem. Chem. Phys. **10**, 4128 (2008).
[25] R. J. Le Roy and J. M. Hutson, J. Chem. Phys. **86**, 837 (1987).
[26] G. Guelachvili, J. Mol. Spectrosc. **79**, 72 (1980).
[27] Y. Z. Zhou, D. Q. Xie, and D. H. Zhang, J. Chem. Phys. **124**, 144317 (2006).
[28] K. Raghavachari, J. A. P. G. W. Trucks, and M. Head-Gordon, Chem. Phys. Lett. **157**, 479 (1989).
[29] D. E. Woon and T. H. Dunning, J. Chem. Phys. **98**, 1358 (1993).
[30] F. M. Tao and Y. K. Pan, Mol. Phys. **81**, 507 (1994).
[31] T. B. Pedersen, B. Fernandez, H. Koch, and J. Makarewicz, J. Chem. Phys. **115**, 8431 (2001).
[32] S. F. Boys and F. Bernardi, Mol. Phys. **19**, 553 (1970).
[33] MOLPRO, a package of *ab initio* programs designed by H. J. Werner and P. J. Knowles, R. D. Amos, A. Berning, D. L. Cooper, M. J. O. Deegan, A. J. Dobbyn, F. Eckert, S. T. Elbert, C. Hampel, R. Lindh, A. W. Lloyd, W. Meyer, A. Nicklass, K. Peterson, R. Pitzer, A. J. Stone, P. R. Taylor, M. E. Mura, P. Pulay, M. Schutz, H. Stoll, and T. Thoorsteinsso.
[34] See supplementary material at http://dx.doi.org/10.1063/1.3428619 for ASCII files containing listings of the *ab initio* points and of the parameters defining the 4D MLR potentials for $v_3=0$ and 1, for a FORTRAN subroutine for generating those 4D potentials, and for a complete listing of all 27 truly bound vibrational levels found for *ortho*-CO_2-H_2.
[35] A. van der Avoird, P. E. S. Wormer, and R. Moszynski, Chem. Rev. (Washington, D.C.) **94**, 1931 (1994).
[36] J. Z. H. Zhang, J. Dai, and W. Zhu, J. Phys. Chem. A **101**, 2746 (1997).
[37] S. Y. Lin and H. Guo, J. Chem. Phys. **117**, 5183 (2002).
[38] G. Audi, A. H. Wapstra, and C. Thibault, Nucl. Phys. A. **729**, 337 (2003).
[39] F. Gatti, C. Lung, M. Menou, Y. Justum, A. Nauts, and X. Chapuisat, J. Chem. Phys. **108**, 8804 (1998).
[40] M. Mladeovic, J. Chem. Phys. **112**, 1070 (2000).
[41] X.-G. Wang and T. Carrington, Jr., J. Tang, and A. R. W. McKellar, J. Chem. Phys. **123**, 034301 (2005).
[42] H.-G. Yu, Chem. Phys. Lett. **365**, 189 (2002).
[43] J. C. Light, I. P. Hamilton, and J. V. Lill, J. Chem. Phys. **82**, 1400 (1985).
[44] R. N. Zare, *Angular Momentum* (Wiley, New York, 1988).

[45] C. Lanczos, J. Res. Natl. Bur. Stand. **45**, 255 (1950).
[46] R. J. Le Roy, N. Dattani, J. A. Coxon, A. J. Ross, P. Crozet, and C. Linton, J. Chem. Phys. **131**, 204309 (2009).
[47] P. Jankowski and K. Szalewicz, J. Chem. Phys. **108**, 3554 (1998).
[48] D. M. Brink and G. R. Satchler, *Angular Momentum* (Clarendon, Oxford, 1975).
[49] A. J. Stone, *The Theory of Intermolecular Forces* (Clarendon, Oxford, 1996).
[50] D. Lawson and J. F. Harrison, J. Phys. Chem. A **101**, 4781 (1997).
[51] A. Haskopoulos and G. Maroulis, Chem. Phys. Lett. **417**, 235 (2006).
[52] B. L. Jhanwar and W. J. Meath, Chem. Phys. **67**, 185 (1982).
[53] R. Bukowski, J. Sadlej, B. Jeziorski, P. Jankowski, K. Szalewicz, S. A. Kucharski, H. L. Williams, and B. M. Rice, J. Chem. Phys. **110**, 3785 (1999).
[54] F. Visser, P. E. S. Wormer, and W. P. J. H. Jacobs, J. Chem. Phys. **82**, 3753 (1985).
[55] A. D. Buckingham, in *Intermolecular Forces*, edited by J. O. Hirschfelder (Interscience, New York, 1967), Vol. 12, Chap. 2, pp. 107–142.
[56] D. M. Bishop and L. M. Cheung, J. Chem. Phys. **72**, 5125 (1980).
[57] R. J. Le Roy, "betaFIT 2.0: A computer program to fit potential function points to selected analytic functions," University of Waterloo Chemical Physics Research Report No. CP-665, 2009, see http://leroy.uwaterloo.ca/programs/.
[58] R. J. Le Roy, J. Mol. Spectrosc. **191**, 223 (1998).
[59] H. Wei, R. J. Le Roy, R. Wheatley, and W. J. Meath, J. Chem. Phys. **122**, 084321 (2005).
[60] K. Patkowski, W. Cencek, P. Jankowski, K. Szalewicz, J. B. Mehl, G. Garberoglio, and A. H. Harvey, J. Chem. Phys. **129**, 094304 (2008).
[61] In contrast, as was shown for the CO_2–$(He)_n$ system, taking account of the fact that the average value of Q_1 changes from $(v_1,v_2,v_3)=(0,0,0)$ to (0,0,1) led to significant improvements in the predicted vibrational frequency shifts for that system. (Ref. 18).